

Supplementary Information for

Enhanced risk of hot extremes revealed by observation-constrained model projections

Claudia Simolo*, Susanna Corti

* Correspondence to: c.simolo@isac.cnr.it

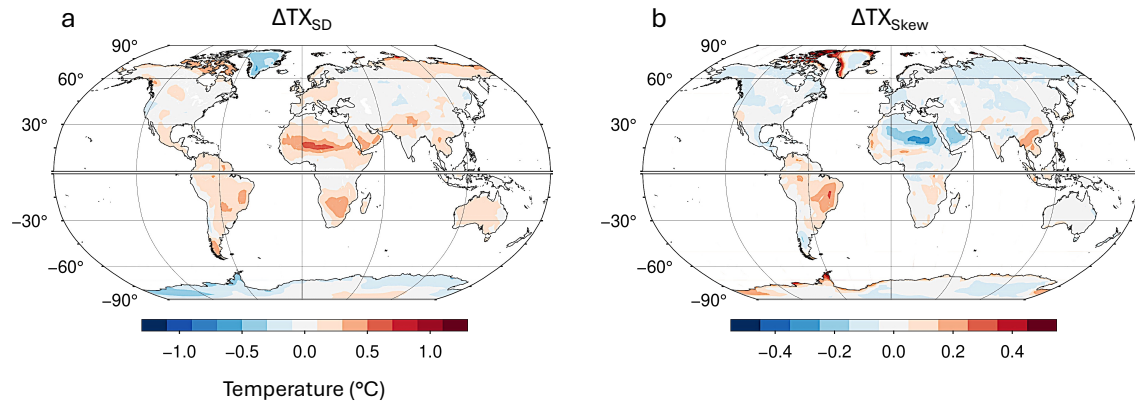
Contents

- Supplementary Table 1
- Supplementary Figures 1 to 10

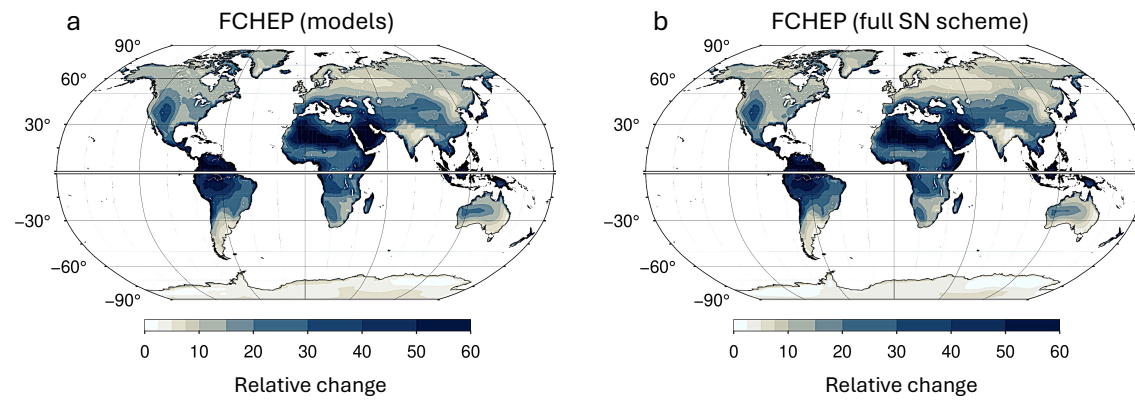
Model list

GCM (Institution)	# lon	x	# lat	$\langle t \rangle_{2^\circ C}$	$\langle t \rangle_{3^\circ C}$
ACCESS-CM2 (CSIRO-ARCCSS)	192	\times	144	2038	2055
ACCESS-ESM1-5 (CSIRO)	192	\times	145	2039	2060
BCC-CSM2-MR (BCC)	320	\times	160	2043	2065
CNRM-CM6-1 (CNRM-CERFACS)	256	\times	128	2040	2058
CNRM-ESM2-1 (CNRM-CERFACS)	256	\times	128	2045	2064
CanESM5 (CCCma)	128	\times	64	2022	2040
EC-Earth3 (EC-Earth-Consortium)	512	\times	256	2036	2055
EC-Earth3-Veg (EC-Earth-Consortium)	512	\times	256	2034	2055
GFDL-ESM4 (NOAA-GFDL)	288	\times	180	2053	2076
HadGEM3-GC31-LL (MOHC)	192	\times	144	2030	2047
INM-CM4-8 (INM)	180	\times	120	2046	2069
INM-CM5-0 (INM)	180	\times	120	2046	2074
IPSL-CM6A-LR (IPSL)	144	\times	143	2034	2050
MIROC6 (MIROC)	256	\times	128	2053	2076
MPI-ESM1-2-HR (DKRZ)	384	\times	192	2049	2073
MPI-ESM1-2-LR (MPI-M)	192	\times	96	2049	2071
MRI-ESM2-0 (MRI)	320	\times	160	2038	2064
NESM3 (NUIST)	192	\times	96	2034	2054
NorESM2-MM (NCC)	288	\times	192	2054	2076
UKESM1-0-LL (MOHC)	192	\times	144	2031	2046

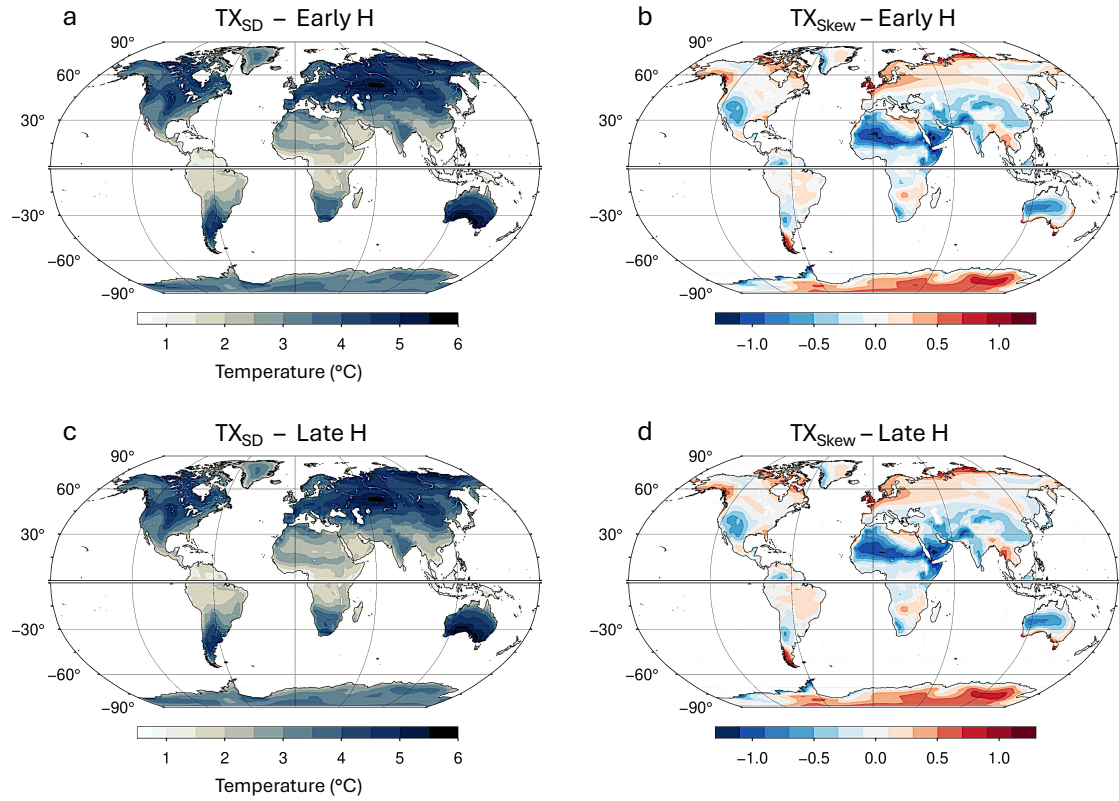
Supplementary Table 1. Details of the CMIP6 simulations used, including model name (institution), horizontal resolution, and approximate timings of crossing relevant levels of GW (2 °C and 3 °C) under the high-forcing scenario SSP5-8.5.



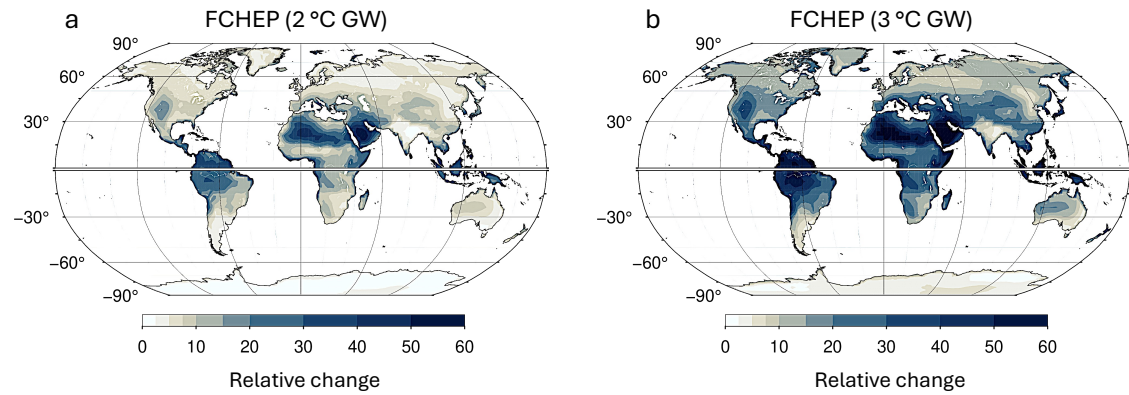
Supplementary Figure 1. Summer changes in TX variability (a) and skewness (b, unitless) at $2\text{ }^{\circ}\text{C}$ of GW, in the mean of model projections over the global land.



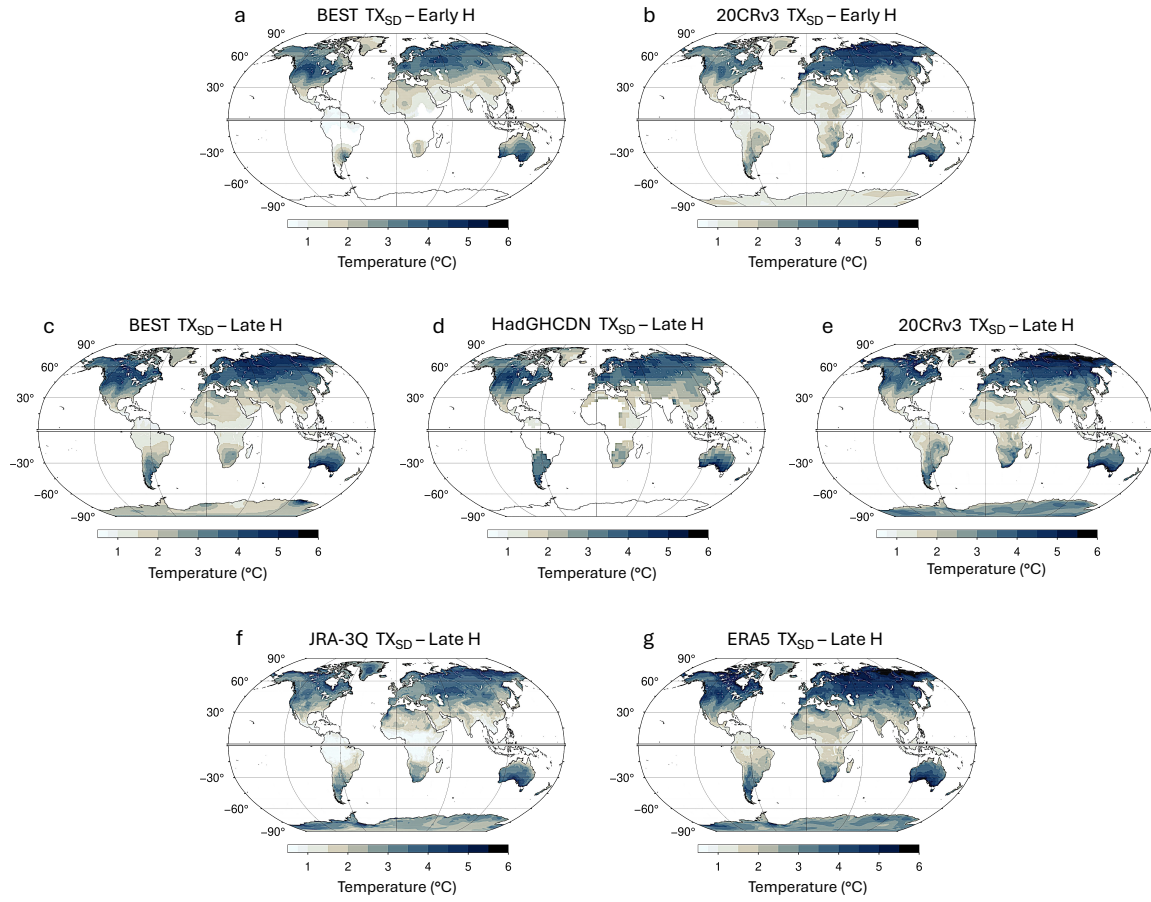
Supplementary Figure 2. Fractional changes in hot event probabilities in the mean of model projections (a) and their theoretical representations in the full SN scheme (b), similar to Fig. 1a,b in the main text but at $3\text{ }^{\circ}\text{C}$ of GW. The theoretically explained fraction (R^2) of the spatial variation in probability changes is approximately 0.98 (0.96–0.99) in the model mean and spread.



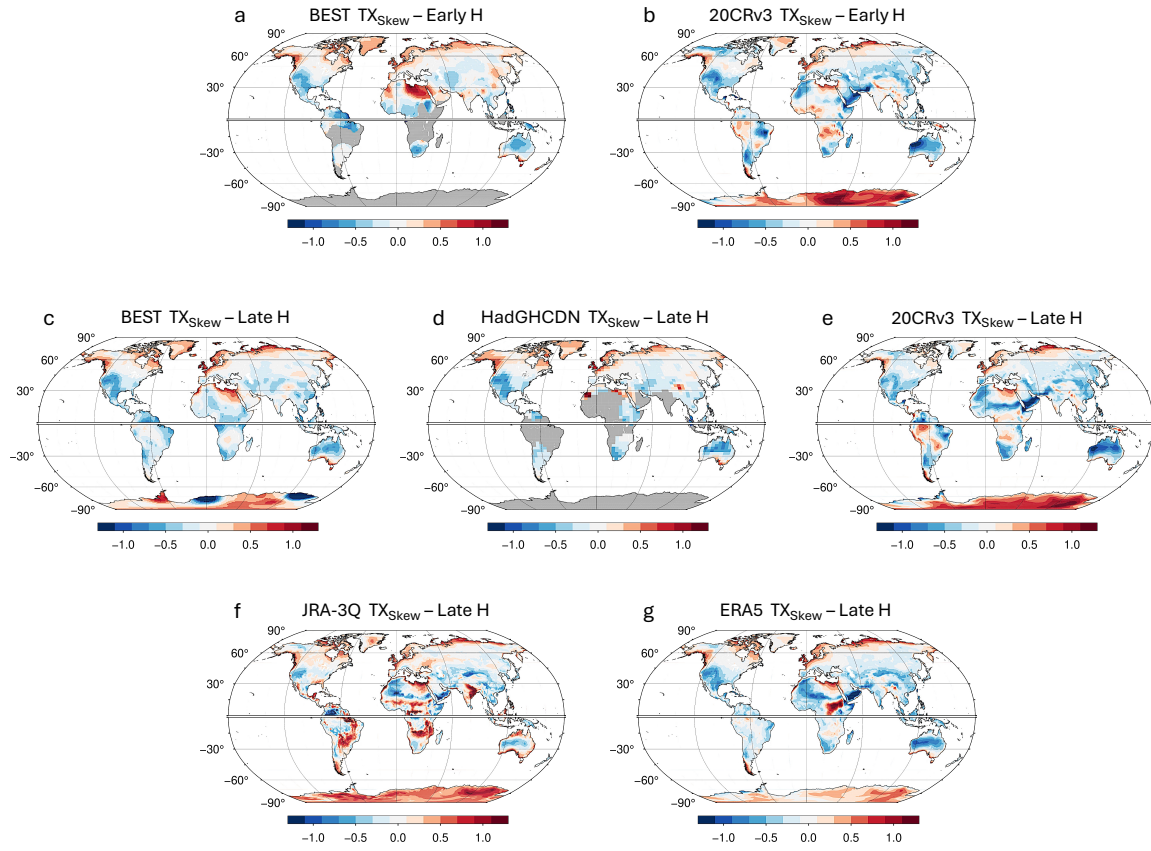
Supplementary Figure 3. a–d Multimodel mean of summer TX variability (**a,c**) and skewness (**b,d**, unitless) for the early (**a,b**) and late (**c,d**) historical periods (1880–1950 and 1951–2000, respectively). TX anomalies are referenced to 1880–1950 climatologies.



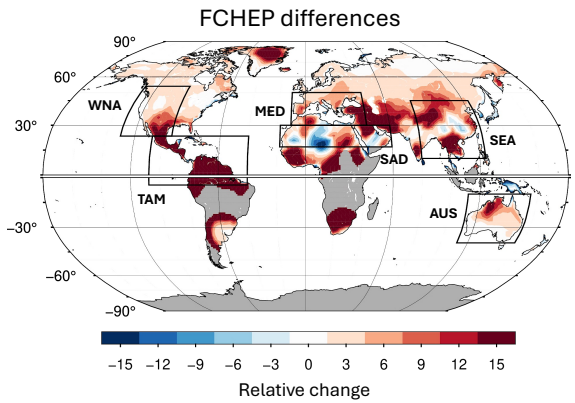
Supplementary Figure 4. Fractional changes in hot event probabilities in the mean of model projections at 2 °C (**a**) and 3 °C of GW (**b**), similar to Fig. 1a (main text) and Supplementary Fig. 2a, respectively, but referenced to the 1880–1950 baseline period.



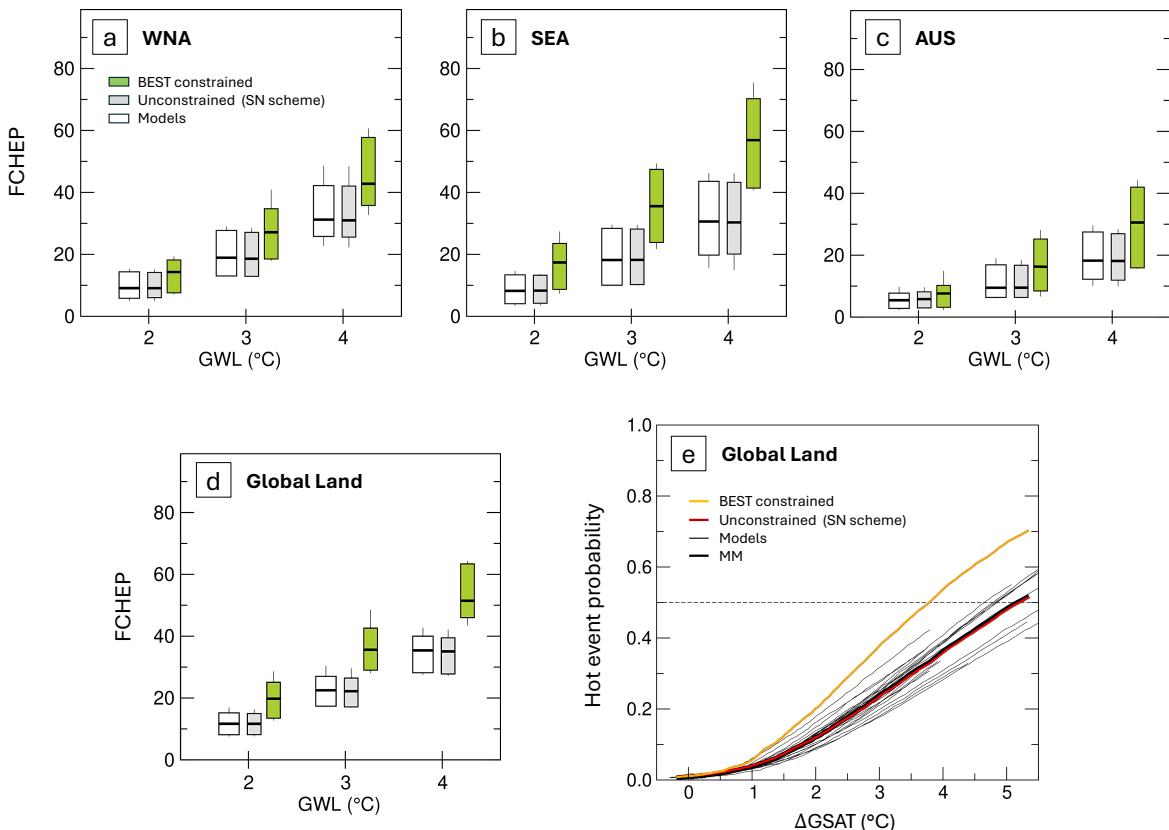
Supplementary Figure 5. a–g Summer TX variability from observational datasets (see Methods in the main text), in the early (**a,b**) and late (**c–g**) historical periods (1880–1950 and 1951–2000, respectively). Blank areas (in panels **a** and **d**) denote insufficient data coverage.



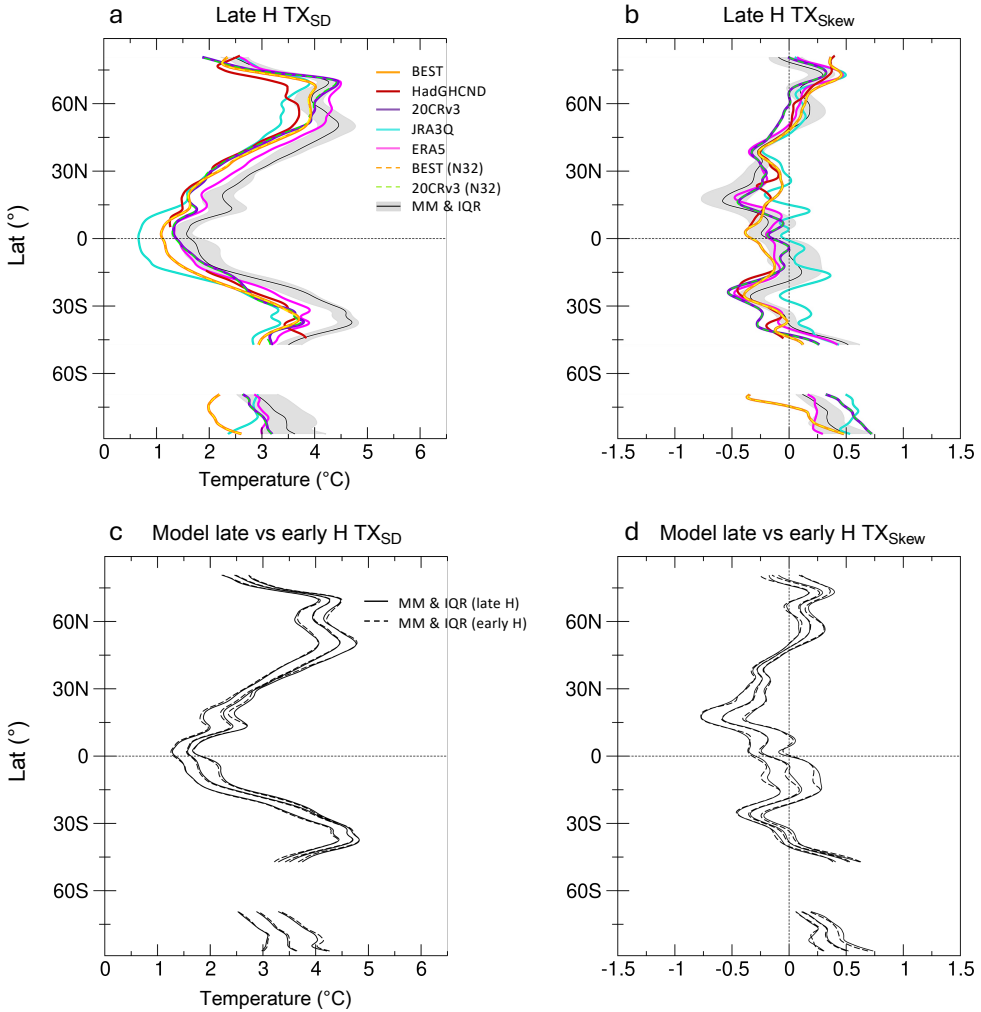
Supplementary Figure 6. a–g Summer TX skewness (unitless) from the observational datasets as in Supplementary Fig. 5, in the early (**a,b**) and late (**c–g**) historical periods (1880–1950 and 1951–2000, respectively). Greyed areas (panels **a** and **d**) denote insufficient data coverage.



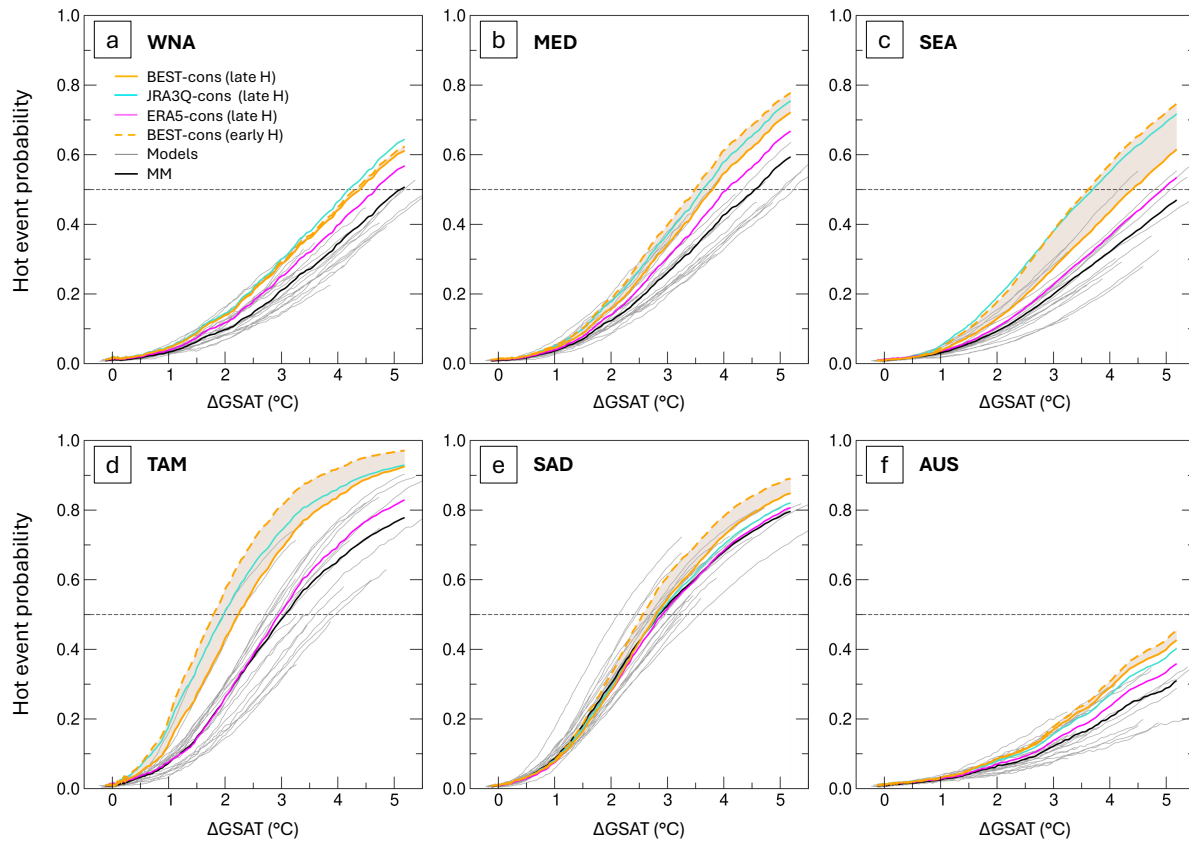
Supplementary Figure 7. Grid-point differences between BEST-constrained and unconstrained model changes (Supplementary Fig. 4a) in hot event probabilities, at 2 °C of GW. Greyed areas indicate gaps in observational coverage.



Supplementary Figure 8. a-d Uncertainties in constrained probability changes (green boxes) compared to those in bare model results and their unconstrained SN representations (white and grey boxes, respectively) for Western North America (**a**), Southeast Asia (**b**), Australia (**c**), and the observed global land (**d**). As in Fig. 5 (main text), boxplots represent the 10th–90th percentile model range, inside bars the median, and whiskers the total spread. **e** Scaling behavior of constrained probabilities (orange line) averaged over the observed global land, compared to bare model results (thick black and thin black lines for the mean and spread, respectively) and their unconstrained SN representation (red line).



Supplementary Figure 9. **a,b** Zonal-mean summer TX variability (**a**) and skewness (**b**, unitless) from the BEST, HadGHCND, and 20CRv3 datasets (solid orange, red, and violet lines, respectively) and model simulations (thin black lines and grey-shaded bands for the MM and IQR, respectively), compared over the late historical period (1951–2000). Additional results from the JRA-3Q and ERA5 reanalyses are also included (light blue and pink lines, respectively). As in Fig. 6 (main text), native-grid TX moments were remapped to a common resolution (N32) before averaging over latitude circles. However, results remain essentially unchanged when temperature fields are remapped to the common grid before calculation of moments, as shown here for BEST and 20CRv3 moments (dashed orange and dashed green lines, respectively) recalculated using this latter approach. **c,d** Model-simulated TX variability (**c**) and skewness (**d**) for 1951–2000 (late H, solid black lines) compared with their counterparts for 1880–1950 (early H, dashed black lines).



Supplementary Figure 10. a-f Scaling behaviour of constrained hot-event probabilities based on the JRA-3Q and ERA5 reanalyses (light blue and pink lines, respectively), for the same regions as in Fig. 7 of the main text. Grey shading denotes the uncertainty range outlined by constrained projections based on BEST late and early historical data (solid and dashed orange lines, respectively). Bare model results are shown as the mean (black lines) and total spread (thin grey lines).